ISBN: 978-628-96613-3-0. ISSN: 2414-6390. Digital Object Identifier: https://dx.doi.org/10.18687/LACCEI2026.1.1.2656

Prototyping a Synergistic Multi-Band UV Device to Enhance the Indoor Air Quality of Hospital Environments

Noel Sánchez[1], Jorge Maldonado[2], Nelson Aguilar[3]
Faculty Mentor: Manuel Adalid Gamero-V[4]
[1,2]Unitec, Honduras, noelsanchez23@unitec.edu, manuelgamero@unitec.edu

Abstract– People spend approximately more than 90% of their time indoors, which exposes them to airborne gaseous and chemical pollutants that can affect their health and well-being. Recent studies have shown that up to 63% of healthcare personnel present at least one health issue associated with poor indoor air quality. Consequently, this study evaluated various existing technologies aimed at improving indoor air quality. Based on the collected information, a synergistic multi-band prototype was developed, harnessing the germicidal efficacy of UV-C light and the photocatalytic effect generated by exposing titanium dioxide to UV-A light. Several tests were conducted under three different experimental scenarios: no intervention, UV-C intervention, and UV-C + photocatalysis intervention. The prototype achieved reductions of 86.19%, 81.68%, and 69.87% in volatile organic compounds, and 100% elimination of aerobic bacteria and yeasts when applied in various hospital environments. The data obtained was subjected to rigorous statistical analysis, demonstrating significant differences (p<0.0001) among each of the experimental scenarios.

Keywords—Computational Fluid Dynamics, HVAC, airborne diseases, infection control, air quality.

I. INTRODUCTION

The rise of industrialization has led to increased emissions of volatile organic compounds (VOCs), resulting in a decline in indoor air quality and adversely affecting individuals within enclosed environments, Moreover, studies have shown that the average person spends approximately 90% of their life indoors [1], thereby increasing exposure to airborne contaminants associated with infections and chronic symptoms, This concern is supported by findings from a study conducted in 148 European office buildings, where 77.7% of occupants reported symptoms related to infections caused by polluted indoor environments [2].

Research trends in indoor air quality have grown exponentially following the COVID-19 pandemic, driven by the need to ensure occupant safety and prevent airborne transmission of microorganisms in enclosed spaces. Among these strategies, the use of ultraviolet (UV) light as a disinfection mechanism has been extensively studied, establishing it a reliable technology for bacterial load reduction.

However, UV light has shown limited efficiency in the removal of VOCs, which restricts its application in comprehensive air disinfection. Alternatively, photocatalysis has emerged as a highly promising method for VOC degradation, applicable in both indoor and outdoor settings.

Therefore, this study aimed to achieve synergistic integration of the technologies to enhance indoor air quality in a hospital environment through the development of a synergistic multi-band prototype. To attain effective synergy, the main components and factors affecting the individual performance of each technology were examined to ensure optimal integration without compromising outcomes, Finally, the impact of the prototype was evaluated by measuring indoor air quality parameters and the inactivation of airborne microorganisms.

II. STATE OF ART

A. Indoor Air Quality

Within healthcare institutions, indoor air quality plays a critical role. Airborne microorganisms typically do not pose a significant threat to healthy individuals. However, pathogenic organisms, along with opportunistic environmental agents, can lead to infections in individuals with compromised immune systems [3]. This also exposes healthcare workers to infections associated with poor indoor air quality. To support this claim, a study was conducted in the intensive care units of two hospitals, revealing that 63% of healthcare workers experienced at least one health issue related to poor indoor air quality [4].

Thus, monitoring indoor air quality in healthcare facilities is a fundamental step in directly addressing the presence and spread of airborne microorganisms involved in healthcare-associated infections [5].

B. UVGI

Ultraviolet Germicidal Irradiation (UVGI) utilizes short-wavelength ultraviolet light (UV-C) to inactive organisms such as viruses, bacteria, and fungi, thereby preventing their reproduction and the spread of diseases [6]. It is important to note that UV-C radiation (wavelength range: 220-280 nm) is employed because it has been proven to be an effective method for eliminating a wide range of microorganisms and viruses [7].

In another study, it was found that the radiation dose required for bacterial inactivation typically ranges from several hundreds to hundreds of mJ/cm^2 [8]. However, the effectiveness of UVGI in removing volatile organic compounds (VOCs) remains limited.

C. Photocatalysis

Another factor affecting indoor air quality (IAQ) is the presence of volatile organic compounds (VOCs), which have been associated with conditions such as asthma, chronic obstructive pulmonary disease, cardiovascular diseases, and gastrointestinal cancers [9]. In this context, a study was conducted that identified the most common VOCs found in indoor environments, while also highlighting the perceived health risks posed by these compounds [10].

As a response to this issue, photocatalysis has emerged as an effective method for degrading a wide spectrum of pollutants and biological agents. Its application has been prioritized using ultraviolet light in ventilation ducts within environments such as hospitals and industrial facilities [8]. In this regard, another study implemented photocatalysis using visible light to activate the photocatalyst or photosensitive surface, given that the setup was deployed in an outdoor setting [11]. Despite employing different approaches, both studies share the same goal: the photocatalytic degradation of VOCs.

III. Methods

The approach of the present research was quantitative in nature, as it was based on the collection and analysis of numeric data related to the effectiveness of the proposed prototype in improving indoor air quality and reducing microorganism counts. Decision-making was also guided by descriptive and inferential statistical analysis.

Dependent and independent variables were selected to structure the study, with the dependent variables being influenced by the manipulation of the independent variables in Fig. 1.

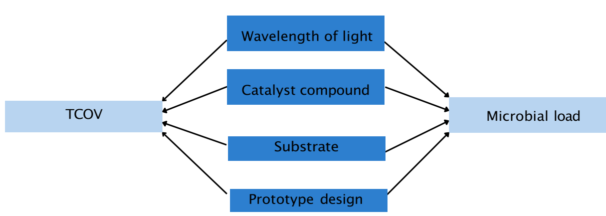

Fig. 1 Dependent and Independent Variables.

A. Techniques and Instruments Applied

This section presents the techniques and instruments used in the development of this project.

- Ansys Fluent Software
- SolidWorks Software
- Datatab Software
- AutoCad Software
- Balometer
- Air Quality Monitor
- Petri Dish
- Flowchart

B. Materials

The following materials were used to construct the synergistic multi-band UV prototype:

- Germicidal UV-C lamp
- Titanium dioxide
- Prototype housing
- Fans
- Battery container
- Aluminum foil
- Plaskolite acrylic sheet

C. Study Methodology

To ensure a direct correlation between each design stage and its corresponding validation phase, the V-model methodology was implemented (Fig. 2). Additionally, the study design was experimental in nature, given the manipulation of independent variables to observe their impact on the dependent variables.

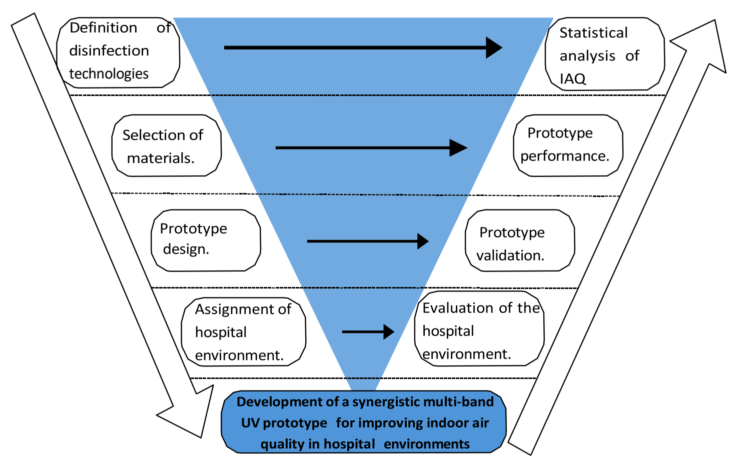

Fig. 2 V-Methodology the left side presents the design steps and the right side the validation steps.

D. Survey and Study of the Assigned Areas

The study was conducted in three areas of the pediatric intensive care unit: the main area, individual cubicle #7, and individual cubicle #8. Due to space constraints, it was not feasible to perform measurements across all ventilation grilles in the different zones; therefore, sampling techniques were applied to obtain an overall estimate of the required data.

Measurements of airflow, ambient temperature, relative humidity, and other values were obtained using specialized instruments and are considered direct measurements. Accordingly, following standard recommendations, the central value of each measurement was determined using the arithmetic mean (1), and the statistical error was calculated using the standard deviation (2).

$$\langle x \rangle = \frac{\sum_{i=1}^{n} x_i}{n} \quad (1)$$

$$\sigma_{ex} = \sqrt{\frac{\sum_{i=1}^{n}(x_i - < x >)^2}{n}} \quad (2)$$

Since access to all ventilation grilles was not available, a statistical calculation for finite populations was performed (3). It was determined that a minimum sample of four grilles would be sufficient to estimate the average airflow with a 95% confidence level.

$$n = \frac{N \cdot z^2 \cdot s^2}{(N-1) \cdot E^2 + z^2 \cdot s^2} \quad (3)$$

This statistical approach ensures a valid statistical representation, allowing the results to be extrapolated to the entire set of grilles that are homogeneous in size and characteristics.

On the other hand, the values for the circular area and air velocity are considered indirect measurements; therefore, the statistical error formula for indirect measurements was applied (4).

$$\sigma_F = \sqrt{\left(\frac{\partial F}{\partial x}\sigma_x\right)^2 + \left(\frac{\partial F}{\partial y}\sigma_y\right)^2} \quad (4)$$

Finally, the collected data were documented for use in the airflow simulation conducted in Ansys Fluent. The measurements yielded ranging from 1.472 2 ± 0.010 m/s to 1.495 ± 0.011 m/s across the various air outlet grilles, and from -0.110 ± 0.005 m/s to -0.112 ± 0.005 m/s in the return grilles.

E. CFD Analysis

Once the boundary conditions of the rooms were defined, the modeling process was carried out as shown in Fig. 3.

The airflow simulation was conducted in Ansys Fluent with the aim of identifying the areas with the highest airflow intensity, to determine the optimal placement of the prototype in Fig. 4.

The standard k-epsilon turbulence model was applied in order to accurately represent the behavior of airflow within the room. The selected turbulence mode is defined by the turbulent kinetic energy equations (5).

$$\frac{\partial}{\partial t}(\rho k) + \frac{\partial}{\partial x_i}(\rho k u_i) = \frac{\partial}{\partial x_j}\left[\left(\mu + \frac{\mu_t}{\sigma_k}\right)\frac{\partial k}{\partial x_j}\right] + G_k + G_b - \rho\varepsilon - Y_m + S_k \quad (5)$$

The dissipation rate (6) was used to identify areas within the room exhibiting stagnant airflow, which served as a basis for exclusion in the prototype placement process.

$$\frac{\partial}{\partial t}(\rho \varepsilon) + \frac{\partial}{\partial x_i}(\rho \varepsilon u_i) = \frac{\partial}{\partial x_j}\left[\left(\mu + \frac{\mu_t}{\sigma_\varepsilon}\right)\frac{\partial \varepsilon}{\partial x_j}\right] + C_{1\varepsilon}\frac{\varepsilon}{k}(G_k + C_{3\varepsilon}G_b) - C_{2\varepsilon}\rho\frac{\varepsilon^2}{k} + S_\varepsilon \quad (6)$$

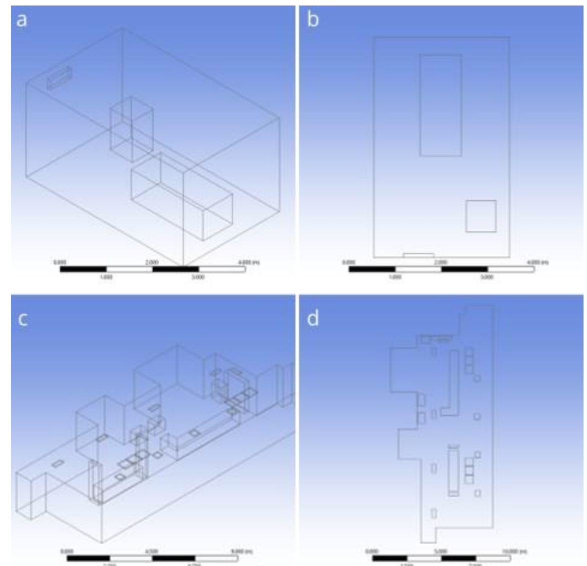

Fig. 3 Room Modeling.

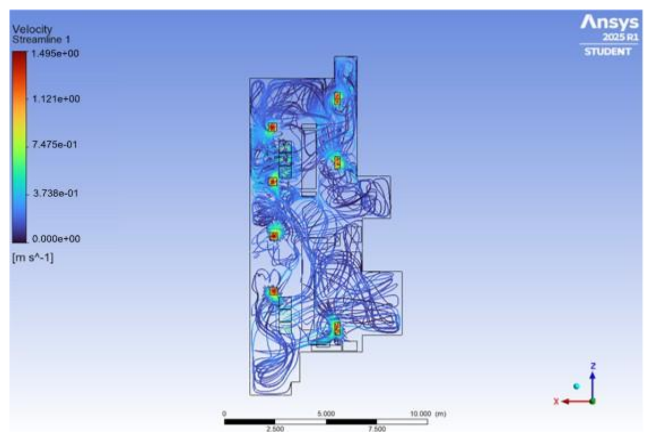

Fig. 4 CFD Simulation.

IV. ANALYSIS AND RESULTS

A. Prototype Validation

1) Prototype Design: A functional prototype was designed with dimensions of 12 x 14 x 61 cm, modeled as an elongated rectangular prism whose cross-section features a modified geometry incorporating an inverted triangular bevel running longitudinally along the entire base of the device. This design aimed to optimize the internal airflow in Fig. 5.

The structured implementation of three progressive experimental scenarios enabled differentiation of the contribution of each treatment mechanism. The baseline condition provided reference environmental values under normal hospital operation. The UV-C-only intervention allowed isolation of germicidal irradiation effects, while the combined UV-C and photocatalysis scenario assessed the complete operational configuration of the prototype. This phased evaluation strategy ensured that the observed improvements could be attributed to the addition of the photocatalytic stage rather than external environmental variation.

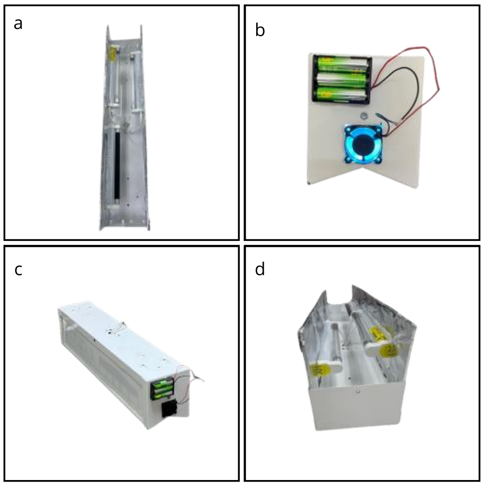

Fig. 5 Prototype of the device.

2) CFD Analysis of Internal Airflow: A computational fluid dynamics simulation was conducted to observe the airflow behavior inside the prototype. Velocity values ranging from 0.0 to 0.307 m/s were obtained in Fig. 7.

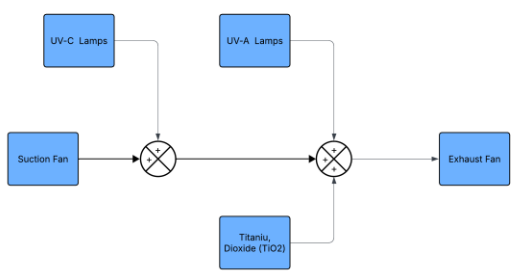

Fig. 6 Block Diagram – Synergistic Multi – Band UV Prototype

To provide a clearer representation of the internal operational sequence of the prototype, a block diagram was developed to illustrate the airflow pathway and the interaction stages occurring within the device. The diagram summarizes the sequential integration of mechanical ventilation, UV-C germicidal irradiation, and UV-A activated TiO_2 photocatalytic oxidation, highlighting the synergistic configuration implemented in the system.

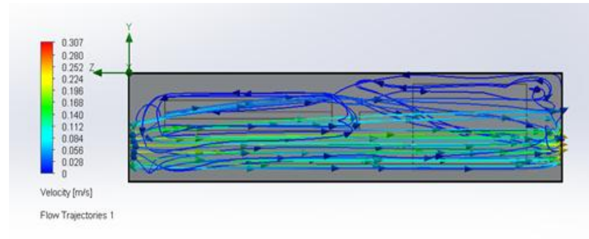

Fig. 7 Flow Analysis Simulation. Blue represents a low velocity; shades of green represent medium velocity and red at a high velocity.

Figure 8 presents the functional architecture of the proposed multi-band UV prototype.

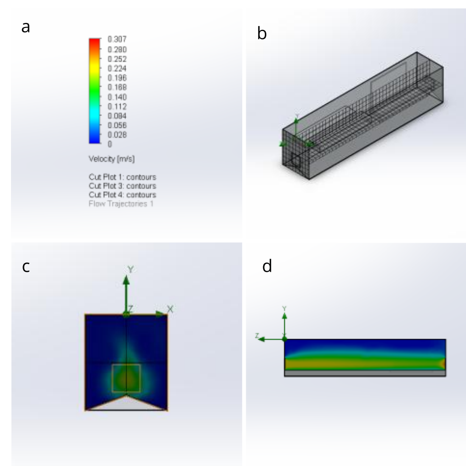

Fig. 8 CFD Analysis of Internal Airflow

3) Mathematical Validation: The validation of the germicidal effect consisted of calculating the UV radiation dose generated by the lamps to be installed (7). The objective was to compare the obtained value with those reported in the literature to assess the capability for microorganism inactivation through radiation.

$$D\left[\frac{mJ}{cm^2}\right] = E\left[\frac{mW}{cm^2}\right]\cdot t\,[s] \qquad (7)$$

Considering that the lamp positioning allows for double exposure to the irradiance values, the emitted radiation can be expected to exceed the calculated dose, as only the dose per lamp was estimated. Furthermore, the highest airflow concentration is found between velocities of 0.168 m/s and 0.224 m/s; therefore, the actual radiation doses should be considered within the range of 3.362 mJ/cm^2, which fall within the acceptable limits for airborne microorganism elimination according to the literature (1-10 mJ/cm^2).

4) Photocatalytic Activation Mechanism: The photocatalytic degradation process is initiated when titanium dioxide (TiO_2), acting as a semiconductor material, is irradiated

with photons whose energy equals or exceeds its bandgap energy (≈3.2 eV for anatase phase). Under UV-A radiation at 365 nm, photons with an energy of approximately 3.4 eV are generated, which is sufficient to promote an electron from the valence band to the conduction band.

This excitation produces electron-hole pairs (e^-/h^+), which subsequently interact with oxygen and water molecules present in the air, forming reactive oxygen species (ROS) such as hydroxyl radicals (OH) and superoxide anions (O_2^-). These highly oxidative species are responsible for the mineralization of volatile organic compounds into carbon dioxide and water.

The incorporation of UV-A radiation in combination with UV-C irradiance enables simultaneous microbial inactivation and VOC degradation within the same airflow pathway, thereby promoting a synergistic disinfection mechanism.

5) UV Dose and Exposure Time Estimation: The UV radiation dose (D) delivered to airborne microorganisms was estimated to be used (8):

$$D = I \times t \tag{8}$$

where I represent the irradiance (mW/cm²) and t corresponds to the exposure time (s).

The irradiance was calculated considering the inverse square law (9):

$$I = \frac{P}{4\pi r^2} \tag{9}$$

where P is the lamp radiant power and r is the distance between the lamp and the airflow pathway.

Given the internal airflow velocity range (0.168–0.224 m/s) and the effective irradiation length inside the prototype, the estimated exposure time ensured a minimum dose within the literature-reported inactivation range (1–10 mJ/cm² for airborne viruses and bacteria). This confirms that the prototype operates within effective germicidal threshold.

TABLE I
TECHNICAL SPECIFICATIONS OF UV LAMPS

Parameter	UV-C Lamp	UV-A Lamp
Wavelength	254 nm	365 nm
Power	6 W	6 W
Supply Voltage	110 V	110 V
Lamp's Length	23.50 cm	23.50 cm
Diameter	3.5 cm	3.5 cm
Irradiance	257,5 $\mu W/cm^2$	N/A

B. *Prototype Performance*

1) Prototype Statistics: Three experimental scenarios were considered: no intervention, UV-C intervention, and UV-C plus photocatalysis intervention. Four measurements were taken for each scenario, documenting the variables of total volatile organic compounds (TVOCs), carbon dioxide, and formaldehyde. The process was repeated in each of the three rooms where the prototype was installed.

Descriptive statistics allowed for the identification of trends in the behavior of the obtained data.

It was found that, without any type of intervention, the average concentration values of TVOCs remained higher ($\bar{x}$ = 0.71850 mg/m³). In contrast, a considerable decrease was observed with the UV-C intervention ($\bar{x}$ = 0.57800 mg/m³), representing a 19.55% reduction. However, VOCs were reduced to a greater extent when the UV-C + photocatalysis intervention was applied, yielding an average value of ($\bar{x}$ = 0.09925 mg/m³), equivalent to an 86.19% reduction in TVOCs.

The variance and coefficient of variation for the data obtained in the experimental scenarios were as follows: without intervention (s^2 = 0.00007, CV = 1.19%), with UV-C intervention (s^2 = 0.00009, CV = 1.60%), and with UV-C + photocatalysis intervention (s^2 = 0.00024, CV = 15.57%). This clearly indicates that, despite achieving lower TVOC levels, the UV-C + photocatalysis intervention produced more variable measurements, which may suggest instability.

The data demonstrated a consistent trend across the different experimental scenarios between the UCIP room and cubicle 7, despite noticeable changes in the measured values. The highest average concentration was observed in the no-intervention scenario ($\bar{x}$ = 0.16925 mg/m³), followed by the UV-C intervention($\bar{x}$ = 0.06625 mg/m³), representing a 60.86% reduction. Lastly, the UV-C + photocatalysis intervention ($\bar{x}$ = 0.031000 mg/m³) corresponded to an 81.68% reduction in TVOCs.

It was observed that the trend in mean values remained consistent, with the highest results recorded without intervention ($\bar{x}$ = 0.2290 mg/m³), followed by the UV-C intervention ($\bar{x}$ = 0.19225 mg/m³), equivalent to a 16.05% reduction, and finally the UV-C + photocatalysis intervention ($\bar{x}$ = 0.06900 mg/m³), equivalent to a 69.87% reduction in TVOCs shown in Fig. 9.

To evaluate the synergistic behavior of the combined UV-C and photocatalysis intervention, the performance of each experimental scenario was compared. While UV-C alone demonstrated partial VOC reduction, the combined intervention produced substantially greater reductions across all evaluated areas.

The enhanced performance suggests that microbial inactivation and photocatalytic oxidation occur simultaneously within the airflow pathway, resulting in a complementary mechanism. UV-C primarily targets nucleic acid damage in microorganisms, whereas UV-A activated TiO_2 promotes oxidative degradation of chemical pollutants.

The observed improvement beyond single-technology intervention supports the hypothesis of synergistic interaction between both mechanisms.

Additionally, descriptive statistical analysis was applied to the results of the bacteriological sampling conducted. It is important to note that the results from cubicle 7 were excluded, as a prior disinfection process had been performed there, which prevented an accurate reflection of the actual conditions. The comparison between experimental scenarios was maintained, yielding positive results shown on Fig. 10.

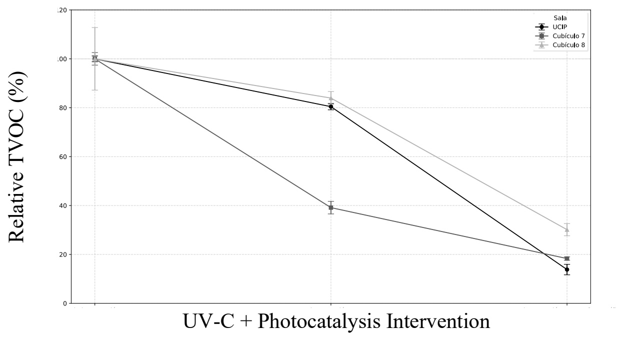

Fig. 9 TVOC Reduction.

Prior to the computational fluid dynamics simulation stage, a geometric modeling phase was conducted to define the internal structural configuration of the prototype. This stage established the spatial arrangement of ultraviolet radiation sources, airflow direction, and photocatalytic interaction surfaces within the confined treatment chamber.

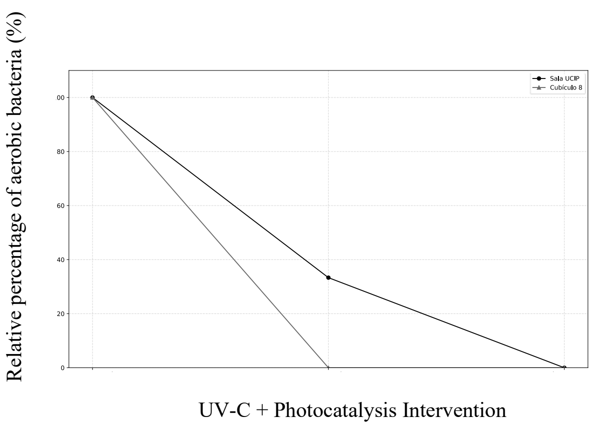

Fig. 10 Aerobic Bacteria Reduction.

The internal geometry was designed considering dimensional constraints previously defined during the prototype fabrication phase. Attention was given to the placement of the UV-C lamps, which were positioned on opposing internal faces to maximize volumetric irradiation and reduce the probability of shadow zones. This opposing configuration promotes cross-irradiation within the airflow channel, increasing the likelihood of microbial exposure to germicidal wavelengths.

Additionally, the UV-A radiation source was strategically located to interact directly with the TiO_2-coated acrylic substrate. The photocatalytic surface was oriented parallel to the airflow direction to ensure prolonged interaction between airborne contaminants and the activated catalytic material. This orientation was selected to increase surface contact probability while maintaining laminar-dominant flow behavior within the chamber.

The geometric definition also considered the effective irradiation distance between lamps and the central airflow pathway. Maintaining controlled separation distances was essential to support subsequent mathematical estimation of radiation dose, as irradiance intensity decreases with distance. By defining fixed spatial parameters during the modeling stage, the system ensured predictable exposure conditions for both UV-C and UV-A radiation zones.

Furthermore, airflow continuity was analyzed conceptually prior to numerical simulation. The configuration aimed to promote linear forced circulation from the suction fan toward the exhaust outlet, minimizing recirculation pockets and stagnation regions. Avoiding turbulent dead zones was a key design objective, as such regions could reduce exposure uniformity and compromise disinfection efficiency.

The geometric modeling stage therefore served as the structural foundation for the entire validation process. It allowed visualization of sequential treatment zones, identification of irradiation overlap regions, and definition of airflow pathway constraints before performing CFD analysis.

Fig. 11 illustrates the internal geometric configuration and spatial distribution of treatment components defined during this modeling phase.

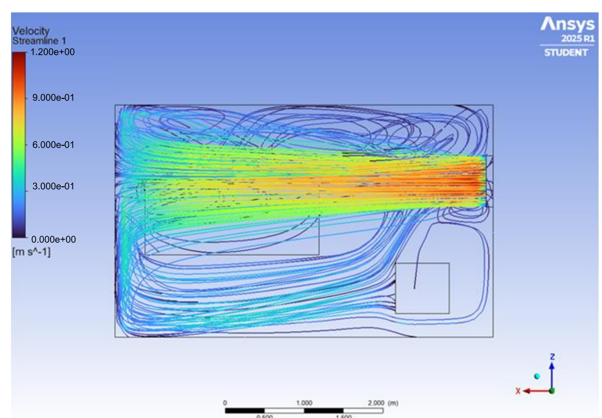

Fig. 11 Internal Geometric Configuration of the prototype prior to CFD Analysis.

The structural representation shown above highlights the sequential arrangement of mechanical and photonic components within a confined irradiation pathway. The configuration demonstrates how ambient air, once drawn into the system, is subjected to controlled exposure within a closed internal volume rather than dispersed within the surrounding environment.

This controlled pathway design enhances predictability in radiation delivery, as the airflow trajectory is constrained by the internal walls and reflective aluminum lining. The reflective surfaces contribute to improved radiation utilization by redirecting stray photons toward the airflow channel, reinforcing the effective irradiance within the treatment chamber.

Moreover, defining the geometry prior to simulation allowed verification of practical feasibility, ensuring that component placement did not obstruct airflow or create mechanical interference between lamps and fans. This step was essential for maintaining operational stability and ensuring that the physical prototype aligned with the intended irradiation model.

By establishing the internal geometric framework before conducting CFD simulation and experimental validation, the study ensured that airflow behavior, radiation exposure, and photocatalytic interaction were structurally integrated rather than independently configured. This integration reinforces the engineered nature of the system and supports the observed performance outcomes reported in subsequent sections.

2) Inferential Statistics: To determine whether statistically significant differences exist between the evaluated groups for the various air quality parameters, analysis of variance was performed using a 95% confidence level. Prior to conducting these tests, assumptions of normality and homogeneity of variances were verified ($p < 0.05$). When both normality and homogeneity of variances were confirmed, the ANOVA test was applied.

However, when the homogeneity of variances assumption was violated but normality was maintained, Welch's ANOVA test was used, as it is appropriate for such data sets. Conversely, if the data did not exhibit a normal distribution, the non-parametric Kruskal-Wallis test was employed.

Finally, the measurement level assumption was met since the independent variable (Type of Intervention) was nominal and the dependent variable (TVOCs) was measurable. Once the measurement level was confirmed, independence of observations was assessed. Due to the experimental methodology employed, measurements across groups did not influence each other, thus fulfilling the independence assumption.

Once the assumptions were confirmed, the corresponding analysis of variance was performed.

3) Significance Tests: The data obtained from the UCIP room were subjected to a one-way ANOVA test, yielding a p-value less than 0.001, leading to the rejection of the null hypothesis. The same result was observed for cubicle 7. In contrast, data from cubicle 8 were analyzed using Welch's ANOVA, also resulting in a p-value less than 0.001.

For each of the variables analyzed-TVOCs, HCHO, and CO2-p-values below 0.001 were obtained, indicating that the prototype has a significant impact.

TABLE II
PICU ANOVA (TVOC)

Source of Variation	Sum of Squares	dF	F	ρ
Type of Intervention	0.84	2	3178.62	<0.001
Residual	0	9	-	-
Total	0.84	11	-	-

TABLE III
CUBICLE ANOVA (TVOC)

Source of Variation	Sum of Squares	dF	F	ρ
Type of Intervention	0.04	2	1581.17	<0.001
Residual	0	9	-	-
Total	0.04	11	-	-

TABLE IV
WELCH'S ANOVA FOR CUBICLE 8 (TVOC)

Test	F	df1	df2	ρ
Welch's Test	406.31	2	5.39	<0.001

Furthermore, the high F-value obtained indicates a substantial difference, suggesting that the prototype's influence was successful.

The results demonstrate statistically significant differences depending on the experimental scenarios. However, to identify which specific scenarios exhibited these differences, post hoc tests were conducted.

4) Post Hoc Tests: Since the analysis of variance revealed significant differences, post hoc tests were conducted, specifically the Bonferroni test. This was done to identify between which groups the differences detected by ANOVA occurred. When comparing the groups in pairs (No Intervention/UV-C, No Intervention/UV-C + Photocatalysis, and UV-C/UV-C + Photocatalysis), p-values less than 0.05 were obtained, indicating that the paired groups were significantly different. However, to confirm the Bonferroni test results, Tukey's and Scheffe's tests were also performed, ´ yielding the same results.

E. *Comparative Performance Analysis*

To further evaluate the performance of the proposed system, a comparative analysis between experimental scenarios was conducted. The baseline condition (no intervention), UV-C-only intervention, and the combined UV-C + photocatalysis intervention were examined to determine the incremental improvement provided by the synergistic configuration.

Across all evaluated areas, the combined intervention consistently demonstrated superior pollutant reduction compared to UV-C alone. While UV-C irradiation effectively contributed to partial VOC reduction through indirect photolytic mechanisms, the integration of UV-A activated TiO2, significantly enhanced degradation efficiency.

TABLE V
POST HOC TESTS FOR PICU (TVOC)

Test	Relation	ρ
Bonferroni	A⇔ B	<0.001
	A⇔ C	<0.001
	B⇔ C	<0.001
Tukey's Test	A⇔ B	<0.001
	A⇔ C	<0.001
	B⇔ C	<0.001
Scheffe Test	A⇔ B	N/A
	A⇔ C	N/A
	B⇔ C	N/A
Fisher's Least Significant Difference (LSD) Test	A⇔ B	<0.001
	A⇔ C	<0.001
	B⇔ C	<0.001

The relative improvement between UV-C-only and combined intervention scenarios suggests that the photocatalytic stage provides an additive oxidative mechanism that complements microbial inactivation. This observation supports the hypothesis that integrating multi-band UV irradiation within a confined airflow channel produces enhanced environmental remediation compared to single-band systems.

C. *Effect Size Estimation*

While statistical significance was confirmed through ANOVA testing, effect size estimation was conducted to quantify the magnitude of the observed differences between intervention scenarios. Statistical significance alone does not indicate the practical relevance of the intervention; therefore, effect magnitude was considered to assess engineering impact.

The substantial reduction percentages observed in the UV-C + photocatalysis scenario suggest a large practical effect. The difference between baseline conditions and the combined intervention indicates that the improvement is not only statistically significant but also operationally meaningful in real clinical environments.

This reinforces that the prototype's performance extends beyond statistical detectability and demonstrates tangible environmental improvement.

To improve clarity and enable direct comparison between scenarios, Table X summarizes the mean TVOC concentrations measured under no intervention, UV-C only, and UV-C + photocatalysis across the evaluated hospital areas. This consolidated view highlights the incremental improvement achieved by integrating the photocatalytic stage.

TABLE VI
OVERALL TVOC PERFORMANCE SUMMARY ACROSS SCENARIOS

Area	Baseline	UV-C Only	UV-C + PCO	Maximum Reduction (%)
PICU	0.71850	0.57800	0.09925	86.19
Cubicle 7	0.16925	0.06625	0.03100	81.68
Cubicle 8	0.22900	0.19225	0.06900	69.87

TABLE VII
MICROBIOLOGICAL REDUCTION SUMMARY (%)

Area	UV-C Only	UV-C + Photocatalysis
PICU (aerobic bacteria)	66.67	100
Cubicle 8 (aerobic bacteria)	100	100
PICU (yeasts)	80	100
Cubicle 8 (yeasts)	100	100

V. DISCUSSION

Unlike previous studies conducted exclusively in simulated environments or controlled chambers [12], this research evaluated the prototype within a real hospital setting, enhancing the external validity of the results and allowing assessment under actual clinical conditions. In addition to measuring gaseous pollutants (TVOC, HCHO, and CO2), microbiological sampling was performed using Petri dishes, addressing limitations found in prior works that omitted biological testing [13]. The implementation of ozone-free UV-C lamps also enables potential large-scale application, as suggested in earlier studies [14].

Nonetheless, technical limitations remain, particularly those related to microbial culture type and concentration [15]. Additional constraints were encountered in the experimental setup, including the inability to fully replicate airflow and microbial conditions of ventilation ducts, short testing duration, and the exclusion of environmental variables such as temperature and humidity, which may affect long-term performance [16]. Furthermore, microbiological data collection was limited by financial constraints. These factors represent the main limitations that may have directly influenced the results.

The selection of the Pediatric Intensive Care Unit as the validation site was not arbitrary but technically justified. As described during the site assessment phase, this area presented a defined duct-based ventilation system and continuous airflow circulation, which facilitated realistic evaluation of the prototype under operational hospital conditions. The decision to test the system in an environment characterized by constant clinical activity and sensitive patients allowed performance assessment under demanding and representative conditions rather than controlled laboratory scenarios. This strengthens the practical relevance of the results and supports the feasibility of implementation in similar hospital environments.

The internal configuration of the prototype was designed to ensure sequential exposure of the airflow to different irradiation stages. As established during the physical modeling phase, the system integrates two opposing UV-C lamps for microbial inactivation, followed by a UV-A irradiation zone interacting with a TiO_2-coated acrylic substrate. This configuration was intentionally arranged to promote homogeneous exposure to multiple wavelengths within a confined channel. The linear airflow generated by axial fans guarantees forced circulation across both treatment zones, minimizing stagnation and reinforcing consistent contaminant interaction with active surfaces.

VI. Design limitations

Although the proposed synergistic multi-band UV prototype demonstrated significant reductions in VOC concentration and airborne microbial load, several design and operational limitations should be acknowledged.

The experimental validation was conducted within a limited evaluation period and under specific environmental conditions. Long-term performance of the photocatalytic surface was not assessed, and factors such as surface fouling, dust accumulation, or material aging may influence efficiency over time. Periodic maintenance may therefore be required to ensure sustained performance.

Additionally, the delivered UV dose is directly influenced by airflow velocity and exposure time. Variations in real-world ventilation systems could modify the interaction time between airborne contaminants and the irradiation chambers, potentially affecting system performance under different installation scenarios.

Relative humidity and environmental variability were not independently controlled during the experimental campaign. These parameters may influence both germicidal irradiation effectiveness and photocatalytic oxidation processes. Future studies should evaluate system behavior under controlled environmental gradients and extended operational cycles.

Despite these limitations, the modular architecture of the prototype provides a controlled irradiation pathway that enhances treatment efficiency while maintaining operational safety.

VII. Conclusions

A prototype was developed with a configuration based on airflow velocities of 0.168 m/s and 0.224 m/s, irradiated by two 6-watt UV-C lamps at short distances (5 cm, 6 cm, and 7 cm), providing sufficient radiation dose to eliminate airborne microorganisms (1–10 mJ/cm2). Additionally, a UV-A lamp with a wavelength of 365 nm was included, emitting 3.4 eV per photon, which is sufficient to overcome the bandgap of titanium dioxide and thereby generate the photocatalytic effect responsible for degrading VOCs. In this way, a synergistic multi-band UV effect was achieved.

Significant differences ($p < 0.001$) were observed between the paired data obtained through intervention with only the UV-C lamps compared to the complete prototype intervention (UV-C + photocatalysis) in the treatment of TVOCs. Higher concentrations were observed in the former system ($\bar{x}$ = 0.57800, 0.06625, 0.19225 mg/m³) compared to the latter (x¯ = 0.09925, 0.031000, 0.06900 mg/m³) in the UCIP room, cubicle 7, and cubicle 8, respectively.

When applying the full intervention (UV-C irradiation + photocatalysis), reductions of 86.19%, 81.68%, and 69.87% in total TVOCs were observed across the three evaluated rooms. This significant difference was further confirmed through various inferential statistical tests applied to each room ($p < 0.001$). Similarly, with the HCHO variable, reductions of 83.40%, 81.18%, and 72.94% were observed when the prototype was applied. Significant differences in these data were also confirmed ($p < 0.005$).

A reduction of 66.67% and 100% in aerobic bacteria presence was achieved in the UCIP room and cubicle 8, respectively, with the application of only the UV-C lamp intervention. In contrast, the full system intervention resulted in a 100% reduction in both rooms. A similar pattern was observed in yeast counts: the UV-C intervention reduced yeast by 80% and 100% in the UCIP room and cubicle 8, respectively, while the UV-C + photocatalysis intervention achieved a 100% reduction in both rooms.

Biosecurity considerations were incorporated into the structural design of the device. As described in the prototype development phase, internal aluminum lining was applied to maximize radiation reflection toward the airflow pathway while simultaneously reducing potential external UV leakage.

References

[1]] Vardoulakis, S., Giagloglou, E., Steinle, S., Davis, A., Sleeuwenhoek, A., Galea, K. S., Dixon, K., & Crawford, J. O. (2020). Indoor Exposure to Selected Air Pollutants in the Home Environment: A Systematic Review. International Journal of Environmental Research and Public Health, 17(23), Article 23. https://doi.org/10.3390/ijerph17238972.

[2] Sakellaris, I., Saraga, D., Mandin, C., de Kluizenaar, Y., Fossati, S., Spinazze, A., Cattaneo, A., Mihucz, V., Szigeti, T., de Oliveira Fer- ` nandes, E., Kalimeri, K., Mabilia, R., Carrer, P., & Bartzis, J. (2021). Association of subjective health symptoms with indoor air quality in European office buildings: The OFFICAIR project. Indoor Air, 31(2), 426–439. https://doi.org/10.1111/ina.12749.

[3] Bonadonna, L., Briancesco, R., Coccia, A. M., Meloni, P., Rosa, G. L., & Moscato, U. (2021). Microbial Air Quality in Healthcare Facilities. International Journal of Environmental Research and Public Health, 18(12), Article 12. https://doi.org/10.3390/ijerph18126226.

[4] Nyembwe, J.-P. K. B., Munanga, J. K., Simoes, N., & da ˜ Silva, M. G. (2024). Ventilation Strategies to Mitigate Air Pollution Impact on Hospital Professionals in Intensive Care Units in the Democratic Republic of Congo. Buildings, 14(7), Article 7. https://doi.org/10.3390/buildings14071996.

[5] do Nascimento, J. P. M., dos Santos, R., dos Santos Silva, M. S., de Araujo, M. A., Anhezini, L., dos Santos, D. ´ E., & da Silva- ´ Filho, E. A. (2023). Indoor Air Contamination by Yeasts in Healthcare Facilities: Risks of Invasive Fungal Infection. Aerobiology, 1(1), Article 1. https://doi.org/10.3390/aerobiology1010002.

[6] Luo, H., & Zhong, L. (2021). Ultraviolet germicidal irradiation (UVGI) for induct airborne bioaerosol disinfection: Review and analysis of design factors. Building and Environment, 197, 107852. https://doi.org/10.1016/j.buildenv.2021.107852.

[7] Lai, P.-Y., Liu, H., Ng, R. J. H., Wint Hnin Thet, B., Chu, H.-S., Teo, J. W. R., Ong, Q., Liu, Y., & Png, C. E. (2021). Investigation of SARS-CoV-2 inactivation using UV-C LEDs in public environments via ray-tracing

simulation. Scientific Reports, 11(1), 22612. https://doi.org/10.1038/s41598-021-02156-8.
[8] Bono, N., Ponti, F., Punta, C., & Candiani, G. (2021). Effect of UV Irradiation and TiO2-Photocatalysis on Airborne Bacteria and Viruses: An Overview. Materials, 14(5), 1075. https://doi.org/10.3390/ma14051075.
[9] Ma, T., Wang, X., He, W., Zhang, G., Shan, T., Song, X., Yang, X., Ma, J., Chen, L., Niu, P., & Chen, T. (2024). Expose to volatile organic compounds is associated with increased risk of depression: A cross-sectional study. Journal of Affective Disorders, 363, 239–248. https://doi.org/10.1016/j.jad.2024.07.028.
[10] Greco, E., De Spirt, A., Miani, A., Piscitelli, P., Trombin, R., Barbieri, P., & Marin, E. (2025). Nanomaterials in Photocatalysis: An In-Depth Analysis of Their Role in Enhancing Indoor Air Quality. Applied Sciences, 15(3), Article 3. https://doi.org/10.3390/app15031629.
[11] Chakravorty, A., & Roy, S. (2024). A review of photocatalysis, basic principles, processes, and materials. Sustainable Chemistry for the Environment, 8, 100155. https://doi.org/10.1016/j.scenv.2024.100155.
[12] Abidi, M., Assadi, A. A., Aouida, S., Tahraoui, H., Khezami, L., Zhang, J., Amrane, A., & Hajjaji, A. (2025). Photocatalytic Activity of Cu2O Loaded TiO2 Heterojunction Composites for the Simultaneous Removal of Organic Pollutants and Bacteria in Indoor Air. Catalysts, 15(4), 360. https://doi.org/10.3390/catal15040360
[13] de Souza, S. O., Cardoso, A. A., Sarmento, A. S. C., & d'Errico, F. (2022). Effectiveness of a UVC air disinfection system for the HVAC of an ICU. European Physical Journal Plus, 137(1), 37. https://doi.org/10.1140/epjp/s13360-021-02240-y
[14] Lee, M., Koziel, J. A., Murphy, W., Jenks, W. S., Chen, B., Li, P., & Banik, C. (2021). Evaluation of TiO2 Based Photocatalytic Treatment of Odor and Gaseous Emissions from Swine Manure with UV-A and UV-C. Animals, 11(5), Article 5. https://doi.org/10.3390/ani11051289
[15] Biasin, M., Bianco, A., Pareschi, G., Cavalleri, A., Cavatorta, C., Fenizia, C., Galli, P., Lessio, L., Lualdi, M., Tombetti, E., Ambrosi, A., Redaelli, E. M. A., Saulle, I., Trabattoni, D., Zanutta, A., & Clerici, M. (2021). UV-C irradiation is highly effective in inactivating SARS-CoV-
[16] J. L. Ordoñez-Ávila, F. Danilo Bonilla and E. D. García, "Development of a teleoperated robot based on an experimental design for sterilization in Honduras," 2021 IEEE International Conference on Machine Learning and Applied Network Technologies (ICMLANT), Soyapango, El Salvador, 2021, pp. 1-6, doi: 10.1109/ICMLANT53170.2021.9690534.